1 **Interaction of modified oligonucleotides with nuclear proteins, formation of novel**

2 **nuclear structures and sequence-independent effects on RNA processing**

3

4 Loren L Flynn #, Ruohan Li # May T Aung-Htut, Ianthe L Pitout, Jack A L Cooper, Alysia

5 Hubbard, Lisa Griffiths, Charlie Bond, Steve D Wilton, Archa H Fox* and Sue Fletcher*

6 **# authors contributed equally**

7 ***corresponding authors**

8 **Abstract (max** 150 words)

9 Oligonucleotides and nucleic acid analogues that alter gene expression are showing

10 therapeutic promise for selected human diseases. The modification of synthetic nucleic acids

11 to protect against nuclease degradation and to influence drug function is common practice,

12 however, such modifications may also confer unexpected physicochemical and biological

13 properties. Here we report backbone-specific effects of modified oligonucleotides on

14 subnuclear organelles, altered distribution of nuclear proteins, the appearance of novel

15 structured nuclear inclusions, and modification of RNA processing in cultured cells

16 transfected with antisense oligonucleotides on a phosphorothioate backbone. Phosphodiester

17 and phosphorodiamidate morpholino oligomers elicited no such consequences. Disruption

18 of subnuclear structures and proteins elicit severe phenotypic disturbances, revealed by

19 transcriptomic analysis of fibroblasts exhibiting such disruption. These data suggest that the

20 toxic effects and adverse events reported after clinical evaluation of phosphorothioate

21 nucleic acid drugs may be mediated, at least in part, by non-specific interaction of nuclear

22 components with the phosphorothioate backbone.

23
24
25 Key Words

26 Antisense oligonucleotides, RNA analogue, RNA processing, paraspeckle proteins, nuclear

27 organelles

28

29 Abbreviations

30 antisense oligonucleotide (AO), spinal muscular atrophy (SMA), Duchenne muscular

31 dystrophy (DMD) phosphorodiamidate morpholino oligomer (PMO) amyotrophic lateral

32 sclerosis (ALS)

33

Introduction

Antisense oligonucleotide drugs are a class of therapeutics designed to alter gene expression and function, and are reported to have delivered therapeutic benefit to spinal muscular atrophy (SMA) type 1 patients (Paton 2017) and a subset of Duchenne muscular dystrophy (DMD) cases (Mendell *et al.* 2013, Mendell *et al.* 2016). *Nusinersen* (*Spinraza*) is a 2′O-methoxyethyl antisense oligonucleotide (AO) on a phosphorothioate backbone, targeting a splice silencer (*ISS-N1*) in *SMN2* intron 7 that promotes exon 7 selection during pre-mRNA splicing (Singh *et al.* 2006) and received Food and Drug Administration (USA) (FDA) approval in December 2016 for the treatment of SMA. *Exondys51* is a phosphorodiamidate morpholino oligomer (PMO) that targets the *DMD* pre-mRNA to exclude exon 51, in order to re-frame the dystrophin transcript around frame shifting deletions flanking exon 51, as a treatment for DMD (Mendell *et al.* 2013). *Exondys51* received accelerated approval from the FDA on September 19th 2016. Other drugs exploiting the antisense concept include Kynamro[®] (mipomersen sodium) (Wong and Goldberg 2014), an adjunctive treatment to reduce LDL-C levels in familial hypercholesteremia, approved in January 2013, followed by an FDA hepatotoxity black box warning; and a number of compounds at various stages of clinical development, predominantly siRNA and oligodeoxyribonucleotide analogues designed to induce RNAse H degradation of target transcripts (for review see (Bennett *et al*. 2017, Stein and Castanotto 2017)). Recently, Alnylam announced the first FDA approval of an RNAi Therapeutic, ONPATTRO™ (patisiran) for the treatment of adult patients with polyneuropathy of hereditary transthyretin-mediated amyloidosis.
(https://www.fda.gov/NewsEvents/Newsroom/PressAnnouncements/ucm616518.htm)

Strategies to improve biological stability and confer pharmaceutical properties to nucleic acid drugs include chemical modifications of the bases and nucleic acid backbone to increase resistance to endogenous nucleases; modifications that influence specific oligomer activity and conjugates that enhance cellular uptake and improve tissue distribution. While the phosphorothioate backbone is the most widely applied chemical modification, changes to the ribose moiety (eg, 2′ O-methylation, 2′ O-methoxyethyl, 2′ O-fluoro), nucleobases and other backbone modifications, including peptide nucleic acids and phosphorodiamidate morpholino oligomers can confer specific characteristics and mechanisms of action (for review see (Veedu 2015, Wilton *et al.* 2015, Tri Le *et al.* 2016)).

67

68   Many laboratories, including our own, routinely use 2´ O-methyl phosphorothioate

69   oligonucleotides to evaluate antisense sequences for targeted splicing modulation, and

70   different modified bases on a phosphorothioate backbone for various other molecular

71   interventions (Lipi *et al.* 2016, Chakravarthy *et al.* 2017). These compounds can be

72   economically prepared in-house and efficiently transfected into a range of cells as cationic

73   liposomes or dendrimer complexes, using commercially available reagents. However, for

74   sustained splice modification, *in vivo* use and clinical application, PMOs have proved safe

75   and effective (Gebski *et al.* 2003, Fletcher *et al.* 2006, Kinali *et al.* 2009, Mendell *et al.*

76   2016). We previously reported that antisense exon skipping sequences prepared and

77   optimized *in vitro* as 2´ O-methyl phosphorothioate oligonucleotides generally perform

78   comparably when synthesized as PMO (Adams *et al.* 2007). An extended antisense sequence

79   targeting the *ISS-N1* region of *SMN2* was validated *in vitro* and *in vivo* using 2´ O-methyl

80   phosphorothioate and PMO chemistries (Mitrpant *et al.* 2013).

81

82   Phosphorothioate backbone modification of nucleic acid drugs is common practice for

83   protection from rapid degradation by circulating and intracellular nucleases, but these

84   modified AOs can interact undesirably with endogenous cellular components. Early work

85   indicated that negatively charged phosphorothioate AOs bind non-specifically to heparin-

86   like proteins, laminin and collagen (Dias and Stein 2002) and more recently,

87   phosphorothioate AOs were reported to interact with nuclear paraspeckle-associated

88   proteins, sequestering them away from their endogenous target, the long non-coding RNA

89   *NEAT1,* and also seeding paraspeckle like-structures in the absence of *NEAT1* (Shen *et al.*

90   2014, Shen *et al.* 2015). Paraspeckles and paraspeckle proteins are involved in

91   transcriptional regulation, transport and splicing pathways (Bond and Fox 2009,

92   Naganuma *et al.* 2012). Beyond the paraspeckle-associated subset (Shen *et al.* 2014),

93   phosphorothioate AOs were also reported to bind an additional approximately 50

94   intracellular proteins (Liang *et al.* 2015) however, these interactions were studied in the

95   context of evaluating the modest impact these interactions had on AO function (Liang *et al.*

96   2015). A broader question relates to the global consequences on cellular processes arising as

97   a result of the interaction of AOs with nuclear proteins.

98

99   Results of *in vivo* studies investigating the consequences of non-specific phosphorothioate

100   AO binding are particularly relevant when considering therapeutic applications. The

101   sequestration of paraspeckle proteins, in particular proteins of the drosophila

102   behaviour/human splicing (DBHS) family, was associated with acute hepatotoxicity,

103   inflammation and apoptosis after application of 2´ fluoro-modified phosphorothioate

104   antisense oligonucleotides with a 5-10-5 gapmer configuration in mice (Shen *et al.* 2018)

105   and while this study focused on the severity of 2´ fluoro-modified phosphorothioate AOs, all

106   2´ modifications evaluated have been shown to sequester paraspeckle proteins, albeit to

107   varying degrees (Shen *et al.* 2014, Liang *et al.* 2015, Shen *et al.* 2018). The backbone-

108   dependent binding of phosphorothioate-modified olionucleotides to platelets *in vitro* and *in*

109   *vivo*, mediated by the platelet-specific receptor glycoprotein VI (GPVI) is also of note (Flierl

110   *et al.* 2015), considering the broad range of nucleic acid therapeutics currently under

111   investigation (for review see (Bennett *et al.* 2017). Oligonucleotides on a phosphorothioate-

112   modified backbone elicited strong platelet activation, signaling, reactive oxygen species

113   generation, adhesion, spreading, aggregation and thrombus formation (Flierl *et al.* 2015). Of

114   particular relevance to current clinical usage, 2´ O-methyl phosphorothioate AOs were

115   reported to activate innate immunity when administered directly to the central nervous

116   system (Toonen *et al.* 2018).

117

118   Here we report that transfection of cultured cells with 2´ O-methyl phosphorothioate

119   antisense sequences resulted in numerous novel, large nuclear inclusions in the form of

120   highly structured fibril-like aggregates that co-stained for the paraspeckle proteins, NONO,

121   SFPQ, PSPC1 and FUS. Other nuclear proteins showed altered distribution in 2´ O-methyl

122   phosphorothioate transfected cells. Intranuclear inclusions begin to form within four hours of

123   transfection, and become dominant structures throughout the nucleus within 24 hours. The

124   inclusions appear stable once formed and may remain evident on the culture substrate, even

125   after death and disintegration of the cell. Transmission electron microscopy on transfected

126   cells revealed numerous large, regular structures reminiscent of amyloid deposits, with

127   electron dense regions. Furthermore, gene ontology analyses following RNA sequencing

128   demonstrated significant disruptions to chromatin silencing; regulation of autophagy;

129   nucleotide excision repair; membrane and organelle organization; apoptosis; signalling and

130   protein transmembrane transport, following 2´ O-methyl phosphorothioate transfection.

131

132

133   **Materials and Methods**

134

4

135 *Antisense oligonucleotides*

136 Phosphorodiamidate morpholino oligomers (PMOs) were purchased from Gene-Tools LLC

137 (Philomath, OR, USA), and 2´ O-methyl phosphorothioate AOs were synthesised by TriLink

138 BioTechnologies (San Diego CA, USA). The following sequences were evaluated; an AO

139 encompassing the *SMN* intron 7 *ISS-N1* target, but with a longer sequence *SMN7D(-10-29)*

140 (5´AUUCACUUUCAUAAUGCUGG 3´); the Gene-Tools standard control oligomer, only

141 known to be biologically active in reticulocytes carrying a splice mutation in the human beta-

142 globin pre-mRNA, as an unrelated sham control AO sequence

143 (5´CCUCUUACCUCAGUUACAAUUUAUA 3´), and identified as 'control AO' throughout

144 this study; *Smn* (5´CAC CUU CCU UCU UUU UGA UU 3´) designed to induce exon mouse

145 *Smn* exon skipping and a *SMN* sense AO (5´ CCAGCAUUAUGAAAGUGAAU 3´)

146 complementary to *SMN7D(-10-29)*.

147

148 *Transfection*

149 The 2´O-methyl phosphorothioate AOs were transfected into dermal fibroblasts as lipoplexes

150 using 3 μl of Lipofectamine 3000 (Life Technologies, Melbourne, Australia) per 1 ml of

151 OptiMEM, according to the manufacturer's protocol. The transfection mix was applied to

152 cells seeded at 10,000 per cover slip for immunofluorescence and 15,000 cells per well in 24

153 well plates for RNA extraction and incubated (37°C) for 24 hours prior to RNA and protein

154 analysis. SMA patient fibroblasts were used for the experiments shown in Figures 1f and 1g

155 (Coriell Cell Repositories, GM03813) and fibroblasts from our in-house biobank, obtained

156 from a healthy volunteer, with informed consent (Murdoch University Human Research

157 Ethics Committee Approval #2013/156) were used for all other experiments, except live-cell

158 imaging (see below).

159

160 PMOs were delivered to cells either uncomplexed (10 μM), annealed to a complementary

161 sense DNA oligonucleotide (phosphodiester leash) and transfected as a lipoplex (200 nM), or

162 by nucleofection using a Nucleofector™ X Unit (Lonza, Melbourne, Australia) according to

163 the manufacturer's instructions. PMOs were delivered using the P2 nucleofection kit and CA-

164 137 program at 1 μM, as determined by the final transfection volume. All PMO transfections

165 were incubated for 72 hours prior to RNA and protein analysis.

166

167 *RT-PCR on AO transfected cells*

168 RNA was extracted using the MagMAX-96 Total RNA Isolation Kit, including DNase

169   treatment (Life Technologies), according to the manufacturer's instructions. RT-PCRs were

170   performed using the One-step Superscript III RT-PCR kit with Platinum Taq polymerase (Life

171   Technologies) according to the manufacturer's instructions. All primer sequences and PCR

172   conditions used in this study are detailed in Supplementary File 1**, Table 1**.

173

174   *cDNA synthesis and quantitative PCR*

175   cDNA was synthesised from (~500 ng) RNA extracted from treated and untreated cell cultures

176   using the Superscript IV first-strand synthesis system (Life Technologies) as per the

177   manufacturer's instructions. Prior to qPCR amplification, cDNA was diluted in RNase/DNase

178   free water (1:5).

179

180   The qPCR reactions were performed using Fast SYBR™ Green Master Mix (ThermoFisher

181   Scientific, Melbourne, Australia) and primers for ribosomal RNA subunits *5S* (100% primer

182   efficiency), *18S* (95% primer efficiency), *45S* (100% primer efficiency) and housekeeping Tata

183   box protein (*TBP;*100% primer efficiency) and beta Tubulin (*TUBB;*94% primer efficiency)

184   transcripts. All primer sequences and cycling conditions used in this study are detailed in

185   Supplementary File 1, **Table 1.** Transcript abundance was measured using the CFX384 Touch™

186   Real Time PCR detection system (Bio-Rad Laboratories Pty., Ltd., Gladesville, Australia). The

187   relative expression of each ribosomal RNA subunit to *TBP* and *TUBB* mRNA was calculated

188   using the $2^{-\Delta\Delta CT}$ method and presented as a fold change compared to untreated cells.

189

190   *Immunofluorescence*

191

192   Approximately 10,000 fibroblasts were seeded onto 22 mm x 22 mm coverslips in

193   6- well plates and incubated for 24 hours, prior to transfection. Following transfection,

194   the cells were fixed using acetone:methanol (1:1) on ice for 4 minutes and air- dried.

195

196

197   Fixed cells were washed in PBS containing 1% Triton X-100 to permeabilise the

198   nuclear membrane, and then in PBS to remove excess Triton X-100. Primary antibodies

199   were diluted in PBS containing 0.05% Tween20 and applied to cells for 1 hour at room

200   temperature. All antibody details and staining conditions are listed in Supplementary File

201   1 **Table 2**. Primary antibodies were detected using AlexaFluor488 anti- mouse (cat no.

202   A11001), anti-rabbit (cat. No A11008) or AlexaFluor568 anti- mouse (cat. No A11004) or

203   anti-rabbit (cat. No A11011) (1:400) after incubation for 1 hour at room temperature, and

204   counterstained with Hoechst 33342 (Sigma-Aldrich) for nuclei detection (1 mg/ml, diluted

205   1:125).

206

207   *Western blotting*

208   Cell lysates were prepared with 125 mM Tris/HCl pH 6.8, 15% SDS, 10% Glycerol, 1.25 μM

209   PMSF (Sigma-Aldrich, NSW, Australia and 1x protease inhibitor cocktail (Sigma-Aldrich)

210   and sonicated 6 times (1 second pulses) before adding bromophenol blue (0.004%) and

211   dithiothreitol (2.5 mM). Samples were heated at 94°C for 5 minutes, cooled on ice and

212   centrifuged at 14,000 x g for 2 min before loading onto the gel.

213

214   Total protein (10 μg), measured by BCA, was loaded per sample on a NuPAGE Novex 4-12%

215   BIS/Tris gel (Life Technologies) and separated at 200 V for 55 minutes. Proteins were

216   transferred onto a Pall Fluorotrans polyvinylidene fluoride (PVDF) membrane at 350 mA for

217   2 hours. Following blocking for 1 hour, the membrane was incubated in 5% skim milk

218   powder in 1x TBST containing the primary antibody diluted as shown in Supplementary File

219   1, **Table 2.** Immunodetection was performed using the Western Breeze Chemiluminescent

220   Immunodetection System (Life Technologies) according to the manufacturer's instructions.

221   Western blot images were captured on a Vilber Lourmat Fusion FX system using Fusion

222   software and Bio- 1D software was used for image analysis.

223

224

225   *Live cell imaging*

226   U2OS cells, previously modified to tag the endogenous SFPQ gene with GFP were used for

227   live-cell imaging (Li *et al.* 2017). Cells were seeded at 1.5 x 10^5 cells per well in a 12-well

228   plate, 24 hours before transfection, with high glucose DMEM (Life Technologies, Cat

229   No.11995065) supplemented with 10% fetal calf serum and 1% penicillin-streptomycin. On

230   the following day, cells in each well were transfected with 100 nM 2′ O-methyl

231   phosphorothioate AOs complexed with 2.2 μl Lipofectamine 3000 following the

232   manufacturer's instructions. Immediately after transfection, the plate was transferred to an

233   Incucyte S3 (Essen Bioscience) for live-cell imaging at 1 hour intervals under 10 x optical

234   zoom. SFPQ-GFP and activated caspase-3/7 were visualised under standard green and red

235   channels. Incucyte Caspase-3/7 Red Apoptosis Assay Reagent (Essen Bioscience, Cat No.

236   4704) was used to reveal cell apoptosis events.

237

238 *High resolution microscopy*

239 SIM imaging was performed using an N-SIM microscope (Nikon Corporation, Tokyo, Japan),

240 with SR Apochromat TIRF 100 x 1.49 NA oil immersion objective. Spherical aberration was

241 reduced using the Ti2 automated correction collar at the beginning of the imaging session.

242 Images were acquired using 405 nm, 488 nm and 561 nm lasers, with stacks of step size 0.12

243 μm (with top and bottom of samples determined visually), using 3D-SIM mode. Images were

244 reconstructed with NIS Elements software (Nikon Corporation, Tokyo, Japan).

245

246 *Transmission electron microscopy*

247 Following transfection, cells were washed in PBS and fixed in cold 2.5% phosphate buffered

248 glutaraldehyde overnight. The fixed cells were scraped and centrifuged, then embedded in 4%

249 agarose. The pellets were processed using a Leica tissue processor, moving through 1%

250 aqueous osmium tetroxide, increasing graded alcohols, propylene oxide, propylene

251 oxide/araldite mix, and finally pure araldite resin. The osmicated cells, surrounded by resin in

252 a beem capsule were polymerised overnight at 80°C to form hard blocks.

253 Semi-thin (0.5 micron) sections were taken from the blocks using glass knives, on an RMC

254 ultratome, and stained with methylene blue (0.1% aqueous Methylene Blue with 0.1%

255 Borax) to visualise available cells. Ultrathin sections were then cut from selected blocks,

256 using a Diatome diamond knife, at approximately 95 nm thickness and mounted on copper

257 mesh grids and stained with uranyl acetate (5% uranyl acetate solution in 5% aqueous acetic

258 acid) and Reynold's lead citrate. The grids were viewed using a JEOL 1400 TEM, at 80 kV

259 and images captured by an 11-megapixel GATAN digital camera at varying magnifications.

260

261 *RNA sequencing and analysis*

262 RNA quality was confirmed using a Bioanalyser (Perkin Elmar, MA, USA) prior to

263 RNAseq. Samples were sent to the Australian Genome Research Facility (AGRF, Perth and

264 Melbourne, Australia) for whole transcriptome library preparation using the TruSeq Stranded

265 Total RNA Library Prep Kit (Illumina, CA, USA) and ribosomal RNA depletion with the

266 Ribo-Zero-Gold kit (Illumina, CA, USA). Sequencing was performed using an Illumina

267 HiSeq 2500 (Illumina, CA, USA) to generate 100 base pair single end reads, resulting in an

268 average 25 million reads per sample. Raw sequencing files were quality checked using

269 FastQC (0.11.7), with all files passing. No adapter contamination was identified, and reads

270 were not trimmed. Transcript quantification was performed with salmon (0.8.2), using an

271 index constructed from the Ensembl GRCh38.93 annotation. Transcript abundance was

8

272   summarised to gene-level counts and imported into R using tximport (1.4.0). Differential

273   expression analysis was performed using DESeq2 (1.16.1) and the default parameters (alpha

274   = 0.1). The heatmap of differentially expressed genes ($p_{adj} < 0.1$) was constructed using the

275   heatmap.2 function from R package gplots (3.0.1). Gene ontology analysis was performed

276   using GSEA (3.0) with 1000 gene set permutations. The gene ontology network was

277   constructed using the Enrichment Map plugin for Cytoscape (3.5.1), with cut-offs: $p < 0.05$,

278   FDR < 0.1 and edge > 0.3.

279

280   **Results**

281

282   *Formation of nuclear inclusions after 2′ O-methyl phosphorothioate AO transfection*

283   The phosphorothioate backbone can interact non-specifically with both intra- and extra-

284   cellular proteins, and recruits paraspeckle proteins and forms paraspeckle-like structures

285   when transfected into Hela cells (Shen *et al.* 2014). However, the dynamics of the formation

286   of these structures, as well as the long-term consequences of these structures on cell

287   physiology remain unknown.

288

289   In this study, we largely focused on two 2′ O-methyl phosphorothioate AOs, one that

290   promotes *SMN2* exon 7 retention during splicing by targeting the *ISS-N1* intronic silencer

291   motif (Singh *et al.* 2006) and the other a control oligomer sequence reported by Genetools

292   LLC and widely used as a transfection control, although additional AO sequences were also

293   tested in some experiments, as indicated below. In order to follow nuclear inclusion

294   formation, we first transfected 2′ O-methyl phosphorothioate AO as lipoplexes (100 nM)

295   into U2OS cells expressing genome engineered GFP-labelled endogenous SFPQ (Li *et al.*

296   2017) and performed live cell imaging over 48 hours (**Figure 1a**). The AO transfection

297   induced formation of nuclear inclusions within 5 hours, and over a period of 12 hours, all of

298   the SFPQ within the nucleus is observed sequestered within the inclusions, as revealed by

299   decreased SFPQ staining of the nucleoplasm. Ultimately, only the inclusions are evident, at

300   which time, the inclusions then coalesce into discrete filaments.

301

302   Immunofluorescent staining of the paraspeckle protein, NONO, showed colocalization in

303   nuclear inclusions in fibroblasts transfected with 2′ O-methyl phosphorothioate *SMN7D(-10-*

304   *29)* sequence at 100 nM concentration, but were also evident at AO concentrations as low as

305   12.5 nM within 24 hours of transfection (**Figure 1b**). Of note, the untreated cells show

9

306   diffuse nucleoplasmic NONO signal, as well as naturally occurring punctate NONO inside

307   endogenous paraspeckle nuclear bodies (Fox *et al.* 2018) (eg. **Figure 1b** (ii)). Nuclear

308   inclusions were also observed following 2′O-methyl phosphorothioate AO transfection into

309   normal human myoblasts, transformed mouse *H2K* myoblasts, and the neuroblastoma SH-

310   SY5Y cell line (Supplementary File 1, **Figure 1).** Once formed, the inclusions appear to be

311   highly stable, and remain evident on the culture substrate following cell death and nuclear

312   fragmentation and blebbing **(Figure 1c (i-ii)).** The nuclear inclusions appear as either long

313   'filaments', punctate foci, or both (**Figure 1c (iii)**). In the past we have routinely observed

314   marked cell death associated with transfection of 2′ O-methyl phosphorothioate AOs into

315   primary cells and cell lines, and hence explored any correlation between cell death and the

316   formation of AO-induced nuclear inclusions. Indeed, we observed here that transfection with

317   2′ O-methyl phosphorothioate AO sequences induced nuclear inclusions that correlated with

318   reduced cell survival (**Figure 1d-e**).

319

320   While transfection of AOs with phosphorothioate and phosphodiester backbones have been

321   demonstrated to result in nuclear inclusions (Shen *et al.* 2014), PMOs are yet to be evaluated

322   in this context. We therefore transfected fibroblasts with the AO sequences described above,

323   synthesized as PMOs. Transfection of the PMO sequences into fibroblasts did not alter the

324   apparent distribution of NONO, nor of any other nuclear proteins studied (**Figure 1f).** In

325   order to demonstrate that poor cellular uptake of these compounds was not a factor, PMOs

326   were transfected using three established delivery techniques known to lead to altered target

327   gene expression; uncomplexed PMO (10 µM), nucleofection (1 µM), and annealed to a

328   complementary DNA "leash" and transfected as a lipoplex (200 nM), all incubated for 72

329   hours after transfection (**Figure 1f (i-iii),** respectively). Immunofluorescent detection of

330   NONO showed no PMO-induced intranuclear inclusion formation or altered distribution of

331   NONO following transfection, under any of the conditions used, and was reproducible,

332   irrespective of the PMO sequence (data not shown). Transfection efficiency and altered exon

333   selection in the target *SMN2* transcript was assessed by RT-PCR across *SMN* exons 4-8,

334   confirming that the absence of intranuclear inclusions in PMO transfected cells was not a

335   consequence of poor uptake of PMO (**Figure 1g**).
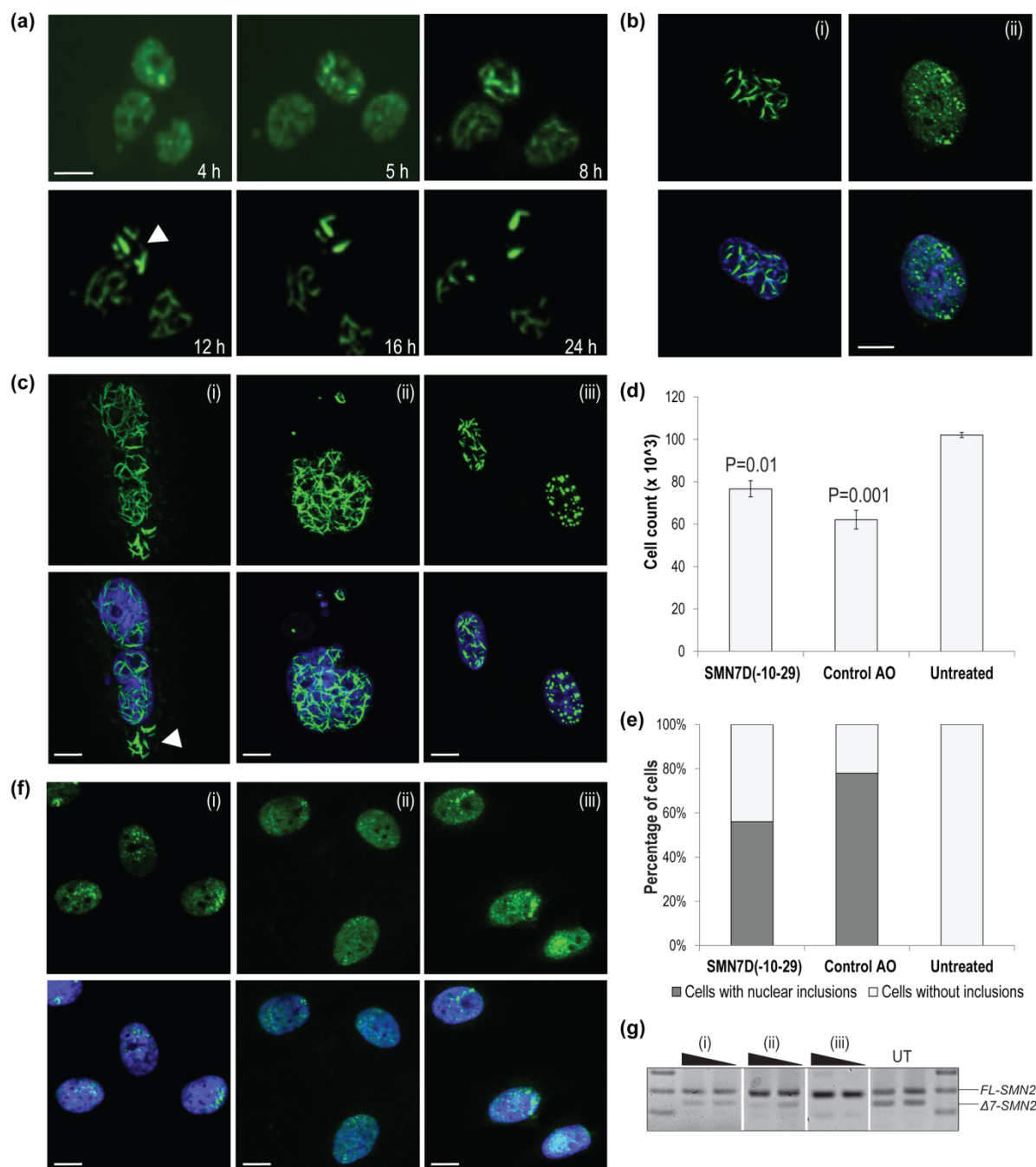
336

337

338

339

340

341

Figure 1 Formation of nuclear inclusions showing **(a)** live cell imaging time-course of U2OS cells with endogenous SFPQ-GFP showing the formation of nuclear inclusions over 24 hours following 2´ O-methyl phosphorothioate control AO transfection (100 nM), inclusions are indicated by the white arrow; **(b)** fibroblasts transfected with 12.5 nM of 2´ O-methyl phosphorothioate *SMN7D(-10-29)* stained for NONO (i), compared to untreated fibroblasts (ii); **(c)** fibroblasts stained for NONO show, (i) nuclear inclusions without evidence of nuclear staining after 2´ O-methyl phosphorothioate *SMN7D(-10-29)* transfection, (ii) nuclear blebbing after 2´ O-methyl phosphorothioate control AO transfection and (iii) nuclear inclusions in the form of filaments or foci induced by transfection with a 2´ O-methyl phosphorothioate *SMN7D(-10-29)* sense sequence AO; **(d)** graph showing the number of viable fibroblasts following 2´ O-methyl phosphorothioate AO transfection (n=4), error bars represent standard error of the mean and P-values calculated using a paired student T-test; **(e)** graph showing the percentage of fibroblasts containing nuclear inclusions following 2´ O-methyl phosphorothioate transfection; **(f)**

353   fibroblasts stained for NONO after transfection with PMO *SMN7D(-10-29)* at (i) high dose un-complexed (10 µM),
354   (ii) using a complementary leash and transfection reagent (200 nM) and (iii) using electroporation (1 µM), all
355   incubated for 72 hours; and **(g)** RT-PCR of full length (FL) and exon 7 skipped (Δ7) *SMN2* transcripts of RNA
356   collected following transfections as in **(f)**. All scale bars = 10 µm.

357

358   To further explore whether AO-induced nuclear inclusions are sequence independent, ninety

359   2′ O-methyl phosphorothioate AOs targeting structural gene transcripts, transcription factors,

360   splicing factors and enzymes, were transfected into fibroblasts and the cells were

361   immunostained for SFPQ (Supplementary File 1, **Table 3**). All AOs tested disrupted SFPQ

362   distribution and all but one AO formed nuclear inclusions by 24 hours following AO

363   transfection at 100 nM, irrespective of length (18-30 bases) and nucleotide composition

364   (Supplementary File 1, **Table 3**), indicating that with optimal transfection efficiency, any 2′

365   O-methyl phosphorothioate sequence is likely to induce nuclear inclusions. One transfected

366   AO induced NONO localization to the nuclear envelope (Supplementary File 1, **Figure 2a**),

367   while a number of AO sequences induced cytoplasmic SFPQ aggregates in addition to

368   nuclear inclusions (Supplementary File 1, **Figure 2b**). The AO-mediated cytoplasmic

369   aggregate formation was also reported by Liang *et al.,* 2014, who observed cytoplasmic

370   structures as a consequence of TCP1-beta subunit interaction with phosphorothioate-AOs in

371   the cytoplasm, in addition to formation of nuclear 'phosphorothioate bodies', and concluded

372   that upon transfection, the TCP1 proteins interact with phosphorothioate AOs and enhance

373   antisense activity (in this case, activation of the RNase H-mediated target degradation)

374   (Liang *et al.* 2015).

375

376   *Composition of nuclear inclusions induced by 2′ O-methyl phosphorothioate AO transfection*

377   The structure and composition of nuclear inclusions was further investigated by

378   immunostaining of additional selected nuclear proteins found in paraspeckles, the nuclear

379   envelope, nucleoli, nuclear speckles, Cajal bodies and nuclear stress bodies. The paraspeckle

380   proteins PSPC1 and FUS were evident in nuclear inclusions (Supplementary File 1, **Figure**

381   **3a and 3b)** and seen to co-localise with NONO and SFPQ positive inclusions (data not

382   shown), while the proteins TDP-43 and hnRNP-A1 were not observed to be components of

383   nuclear inclusions (Supplementary File 1, **Figure 3c and 3d).**

384

385   Coilin, a component of nuclear Cajal bodies, shows altered distribution in 2′ O-methyl

386   phosphorothioate control AO transfected cells and is distributed evenly through the

387   nucleoplasm and cytoplasm of transfected cells showing NONO-positive nuclear inclusions,

388

389
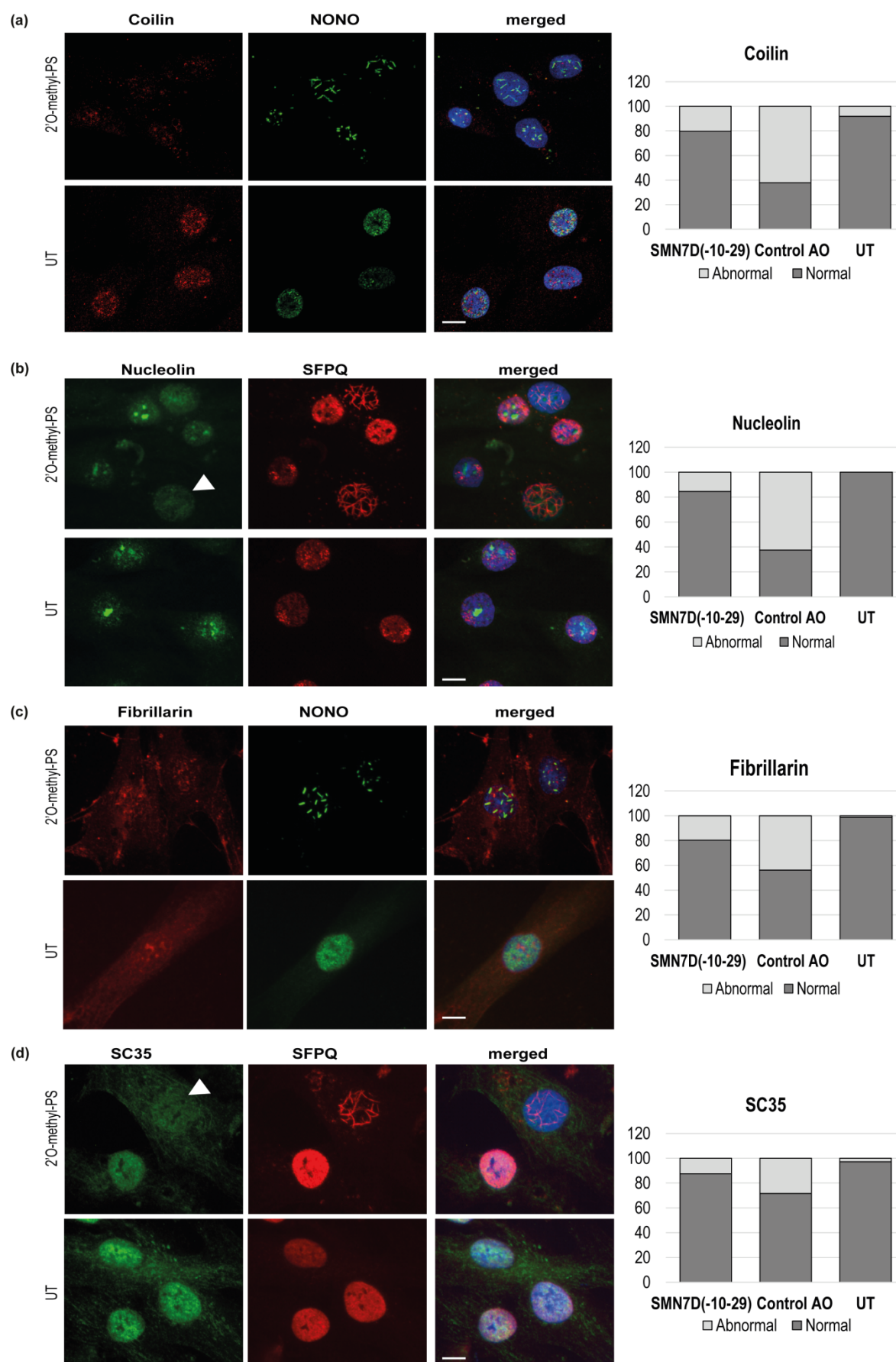
390   **Figure 2** Staining of nuclear bodies following 2´O methyl phosphorothioate transfection (100 nM, 24 hours), with
391   AOs as indicated in cells; **(a)** transfected with the control AO showing coilin (green) and NONO (red) overlayed
392   with hoechst (blue), and graph showing the percentage of abnormal and normally stained cells in cultures
393   transfected with *SMN7D(-10-29)* and control AOs; **(b)** transfected with *SMN7D(-10-29)* showing nucleolin (green)
394   and SFPQ (red) overlayed with hoechst (blue), and graph showing the percentage of abnormal and normally
395   stained cells in cultures transfected with *SMN7D(-10-29)* and control AOs*;* **(c)** transfected with the control AO
396   showing fibrillarin (green) and NONO (red) overlayed with hoechst (blue), and graph showing the percentage of
397   abnormal and normally stained cells in cultures transfected with with *SMN7D(-10-29)* and control AOs and **(d)**
398   transfected with *SMN7D(-10-29)* showing SC35 (green) and SFPQ (red) overlayed with hoechst (blue), and
399   graph showing the percentage of abnormal and normally stained cell in cultures transfected with *SMN7D(-10-29)*
400   and control AOs. All scale bars = 10 µm.
401

402   whereas it is present almost exclusively in the nucleus of untreated cells (**Figure 2a).**

403   Nucleolin and fibrillarin, both markers for the nucleolus, show altered distribution in nuclear

404   inclusion-containing cells, changing from nucleolar to diffuse nucleoplasmic, as shown in

405   **Figures 2b** and **2c**, respectively. The splicing factor and component of nuclear speckles,

406   SC35, showed enhanced cytoplasmic localisation in cells that also contained nuclear

407   inclusions, revealed here by SFPQ immunofluorescence (**Figure 2d**).

408

409   The percentage of AO transfected cells showing disrupted staining or abnormal localization

410   of coilin, nucleolin, fibrillarin and SC35 staining correlated with cells containing

411   intranuclear inclusions, as indicated in the graphs (**Figure 2a-d**). Line intensity profiling

412   shows altered distribution of these nuclear proteins in individual cells that have nuclear

413   inclusions, and is presented in Supplementary File 1, **Figure 4.** Since components of

414   subnuclear organelles were disorganised following transfection with phosphorothioate AOs,

415   the levels of these proteins in the transfected cells were investigated. Western blot analysis

416   showed that the overall abundance of each protein studied to be essentially unchanged

417   following AO transfection. Representative western blots probed for SFPQ, NONO, TDP43,

418   hnRNP-A1, NCL, HSF1 and beta actin, are shown in Supplementary File 1, **Figure 5**.

419

420   *Morphology of 2´ O-methyl phosphorothioate AO-induced nuclear inclusions*

421   Detailed analysis of the 2′ O-methyl phosphorothioate *SMN7D(-10-29)*AO-induced nuclear

422   inclusions was performed using transmission electron microscopy (TEM) on ultra-thin,

423   osmium stained sections (**Figure 3a(i-vi))**. The nuclear inclusions appeared to be

424   microfibrillar or amyloid-like, approximately 200-250 nm in diameter, occurring mostly in

425   groups or bundles. For reference, the width of a DNA double helix is ~2 nm. If captured in a

426   suitable plane of section, the structures appear to have very electron dense termini. Such

14

427   nuclear inclusions have never before been revealed by transmission electron microscopy in

428   the investigating laboratory. The electron dense regions are reminiscent of perichromatin in

429   size and electron density, the inclusions revealed by TEM extend to ~ 2000 nm in length.

430   Numerous small, partially formed inclusions are also evident in nuclei of transfected cells

431   when viewed at higher magnification (**Figure 3a (iii)**).

432

433   Since transmission electron microscopy can only capture segments of the presumed large

434   fibril-like nuclear inclusions, super resolution microscopy was used to examine 2′ O-methyl

435   phosphorothioate *SMN7D(-10-29)* AO transfected and untreated fibroblasts (**Figure 3b-c**).

436   AO transfected fibroblasts co-stained for NONO and SFPQ show a network of many nuclear

437   inclusions characterised by co-localisation of the two proteins, whereas the untreated cells

438   show more even, punctate distribution within paraspeckles (**Figure 3b (i, ii),** respectively).

439   Transfected fibroblasts co-stained for SFPQ and FUS reveal large interconnected fibril-like

440   structures decorated with FUS at mid-points and at the termini (**Figure 3c (i)**). SFPQ, NONO

441   and FUS are all sequestered to the nuclear inclusions, unlike the even nuclear distribution of

442   these proteins in untreated cells (**Figure 3c (ii)**).

443

444   The nuclear envelope protein, lamin B1 showed altered distribution in a proportion of 2′ O-

445   methyl phosphorothioate *SMN7D(-10-29)* transfected cells that exhibited nuclear inclusions

446   (**Figure 3d (i-ii)**). In these cells, the nuclear envelope labelled by immunostaining of lamin

447   B1 appears multi lobular and distorted, reminiscent of those found in the premature ageing

448   disease progeria and in E145K cells (Taimen *et al.* 2009). A single z-frame image is shown

449   in **Figure 3d (i)** that clearly illustrates lamin B1 localized in 4 distinct nuclear lobules.

450   **Figure 3d (ii and iii)** shows the composite image and an image of an immunostained,

451   untreated fibroblast. In all images (**Figure 3b-d**), the nuclear inclusions appear to reside

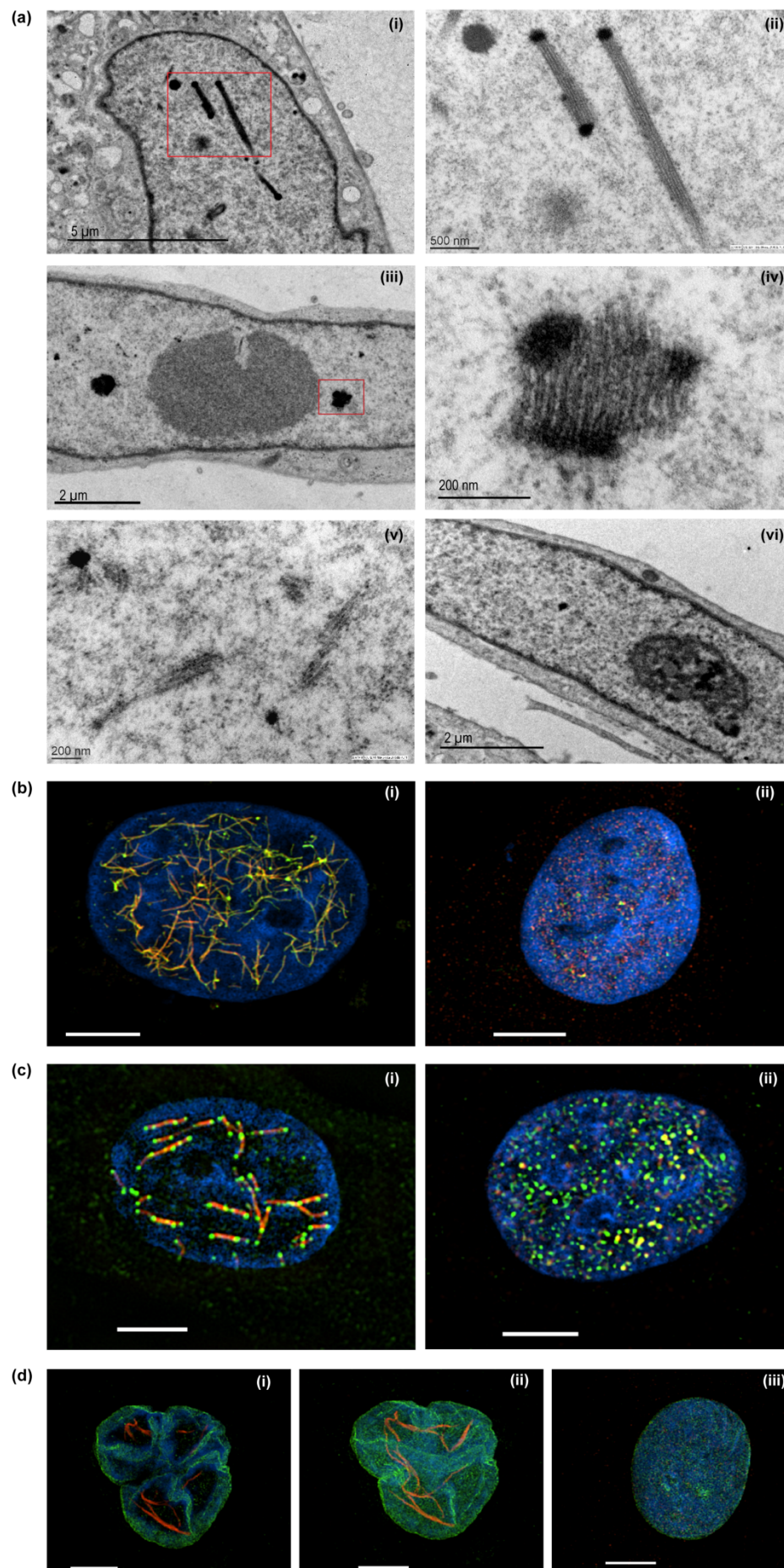452   between areas that may reflect chromosomal territories.

15

453

16

454　**Figure 3** Structural analysis of nuclear inclusions in 2′ O-methyl phosphorothioate *SMN7D(-10-29)* transfected
455　fibroblasts (100 nM, 24 hours), showing **(a)** transmission electron microscopy of (i) nucleus with filament-like
456　nuclear inclusions (scale = 5 µm), (ii) higher magnification of (i) (scale = 500 nm), (iii) nucleus with foci-like
457　nuclear inclusions (scale = 2 µm), (iv) higher magnification of (iv) (scale = 200 nm), (v) partially formed nuclear
458　inclusions (scale = 200 nm), and (vi) untreated nucleus (scale = 2 µm); **(b)** super resolution fluorescence
459　microscopy of SFPQ (green) and NONO (red) co-staining following 2′OMethyl transfection (i) and an untreated
460　cell (ii); **(c)** super resolution fluorescence microscopy of SFPQ (red) and FUS (green) co-staining following
461　transfection (i) and an untreated cell (ii); **(d)** super resolution fluorescence microscopy of NONO (red) and
462　LAMIN-B1 (green) co-staining following transfection (i-ii) and an untreated cell (iii). A single z-frame is shown in (i)
463　and a maximum intensity z-stack in (ii). For all SIM images scale bar = 5 µm.

464

465　*2′ O-methyl phosphorothioate AOs affect ribosomal RNA processing and maturation*

466　Since Cajal bodies and fibrillarin are important in ribosomal RNA processing and assembly,

467　we assessed rRNA levels in 2′ O-methyl phosphorothioate AO transfected cells and

468　untreated cells. qPCR and bioanalyser data show unprocessed rRNA was markedly increased

469　by 2′ O-methyl phosphorothioate AO transfection in fibroblasts (**Figure 4**). A Bioanalyser

470　RNA trace from 2′ O-methyl phosphorothioate control AO transfected fibroblasts (**Figure

471　4a**) showed low levels of 18S and 28S ribosomal subunits, as well as a number of

472　intermediate peaks compared to that on RNA from untreated fibroblasts (**Figure 4b**),

473　consistent with incomplete rRNA processing. Poor RNA quality was ruled out, given a

474　similar pattern was observed in all experimental repeats (n=6). This observation was

475　supported by qPCR analysis of rRNA levels showing a 2 to 3.5-fold increase in the level of

476　the unprocessed 45S rRNA in 2′ O-methyl phosphorothioate transfected compared to

477　untreated fibroblasts (**Figure 4c**). Unprocessed rRNA accumulated over time, following the
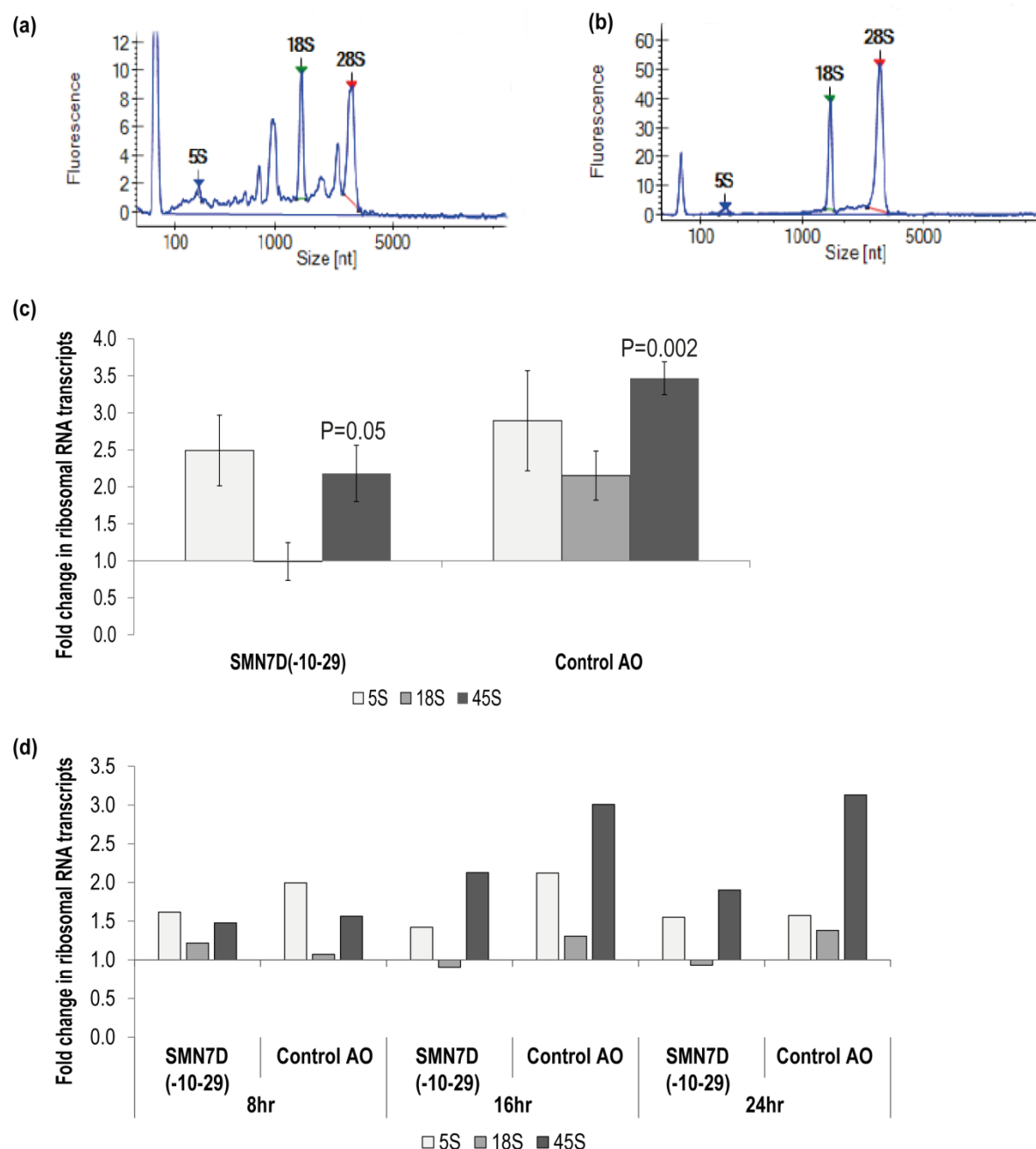
478　formation of nuclear inclusions (**Figure 4d**).

17

479

Figure 4 Analysis of ribosomal RNA processing, showing bioanalyser trace of rRNA from **(a)** 2′O-methyl phosphorothioate control AO transfected cells, and **(b)** untreated cells; **(c)** qPCR analysis of 5S, 18S and 45S rRNA levels following 2′O-methyl phosphorothioate transfection (24 hours). rRNA levels were normalised against *TBP* and compared to those in untreated cells where untreated = 1 (n=3). Error bars represent the standard error of the mean, and P-values were calculated using a paired student T-test; and **(d)** qPCR analysis of rRNA levels over 8, 16 and 24 hours; analysis as in **(c)** (n=1)**.**

2′ O-methyl phosphorothioate AO transfection promotes apoptosis

Following phosphorothioate AO transfection of U2OS cells at 100 nM, live cell imaging was undertaken to evaluate caspase activation (**Figure 5a**). Nuclear inclusions were observed
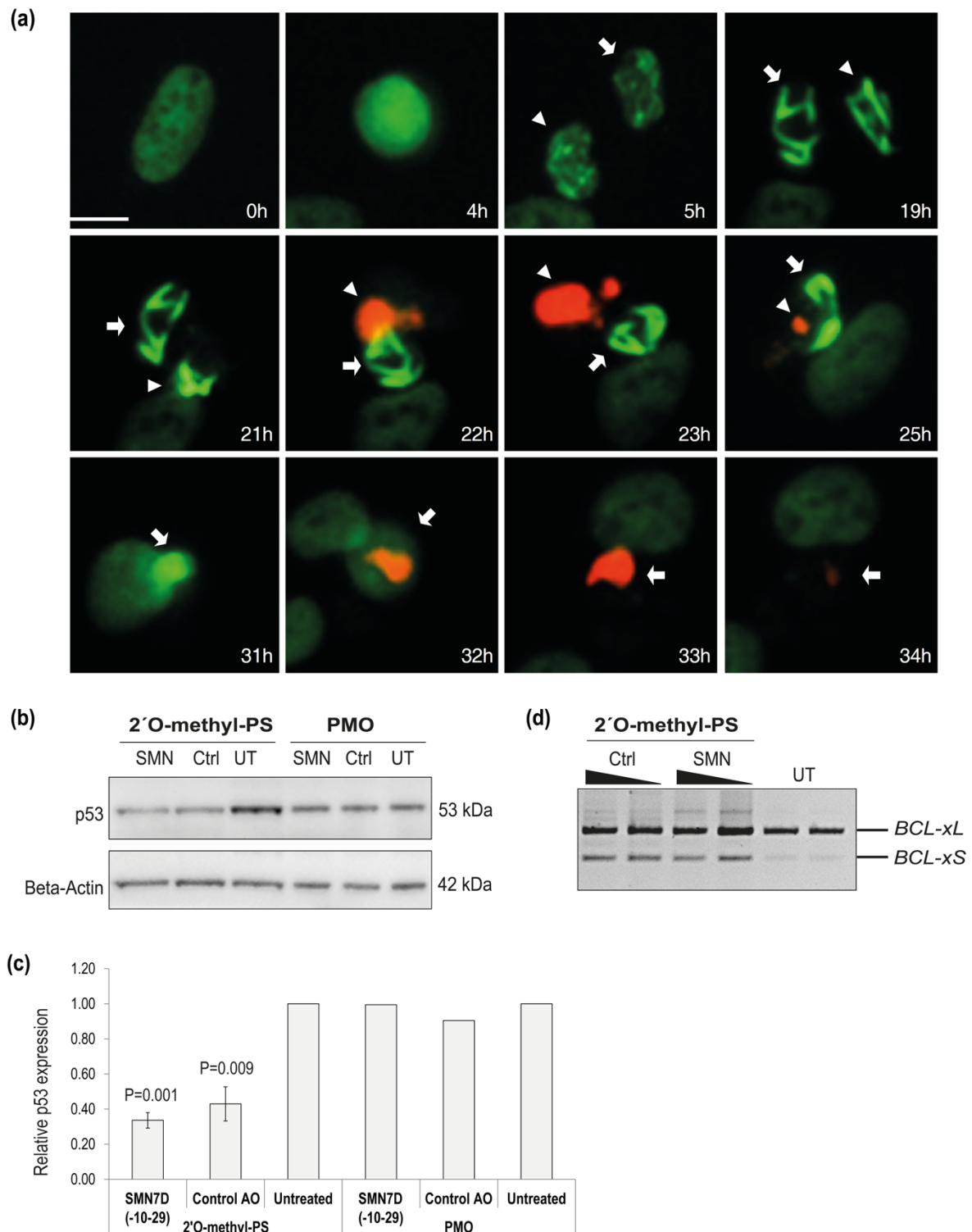
18

490

Figure 5 Analysis of cellular toxicity, showing **(a)** live cell imaging over time of U2OS cells with endogenous SFPQ-GFP (green) transfected with the 2′O-methyl phosphorothioate control AO and stained for caspase 3/7 activation (red). Two sister cells are annotated with arrows, and scale bar = 10 μm; **(b)** western blot of P53 and β-actin levels following 2′O-methyl phosphorothioate AO (n=3) and PMO transfection (n=1); **(c)** densitometry analysis of **(b)** where P53 levels are normalized to β-actin and compared to those in untreated cells where untreated = 1. Error bars represent the standard error of the mean and P-values were calculated using a paired

19

497   student T-test; and **(d)** RT-PCR analysis of *BCL2* transcripts following 2´O-methyl phosphorothioate AO
498   transfection, as indicated at 100 and 50 nM (24 hours).

499

500   after 5 hours in two sister cells. Nuclear inclusions became larger and more compact

501   overtime, followed by caspase activation after 22 hours. No caspase activation was observed

502   in the absence of intranuclear inclusions, identifying nuclear inclusion as complicit in

503   caspase activated apoptosis, leading to cell death. The tumour suppressor protein p53 was

504   decreased, following transfection with 2´ O-methyl phosphorothioate AOs, relative to

505   untreated control cells (**Figure 5b and c**), suggesting that the cell death observed was p53

506   independent, contrary to the findings by Shen *et al.,* 2018 (Shen *et al.* 2018) when using a 2′

507   fluoro-modified AO on a phosphorothioate backbone in the mouse. In comparison to

508   phosphorothioate AO transfection, p53 levels remained unchanged following PMO

509   transfection (**Figure 5b and c**).

510

511   The mitochondrial membrane and apoptosis regulating, *BCL2*-like gene encodes two

512   alternatively spliced, functional protein isoforms, a longer anti-apoptotic isoform BCL-xL,

513   and a shorter pro-apoptotic isoform BCL-xS. Increased abundance of the BCL-xS isoform

514   induces cytochrome C release from the mitochondria, initiating caspase activated apoptosis.

515   RT-PCR across the *BCL* transcripts (**Figure 5d**) shows 2´ O-methyl phosphorothioate AO

516   transfection induces non-specific alternative splicing, increasing the levels of the pro-

517   apoptotic *BCL-xS* transcript, potentially initiating the caspase activation shown in **Figure 5a**.

518

519   *Transcriptome analysis of 2´ O-methyl phosphorothioate transfected cells reveals global*

520   *cellular disruptions*

521   We next evaluated the effect of 2´ O-methyl phosphorothioate transfection and nuclear

522   inclusion formation on the transcriptome by RNA-seq. We prepared RNA from fibroblasts

523   transfected with the two 2´ O-methyl phosphorothioate AOs used throughout this study as

524   well as two control samples (untreated cells and cells transfected with a DNA phosphodiester

525   AO (DNA control) version of the same sequence as the control AO, 100 nM for 24 hours) for

526   RNAseq analysis (n=3). The RNAseq data is available

527   at https://www.ncbi.nlm.nih.gov/geo/query/acc.cgi?acc=GSE121713 (accession number:

528   GSE121713). An RNAseq heatmap comparing the expression of transcripts in 2´ O-methyl

529   phosphorothioate AO transfected fibroblasts to that in cells transfected with the DNA

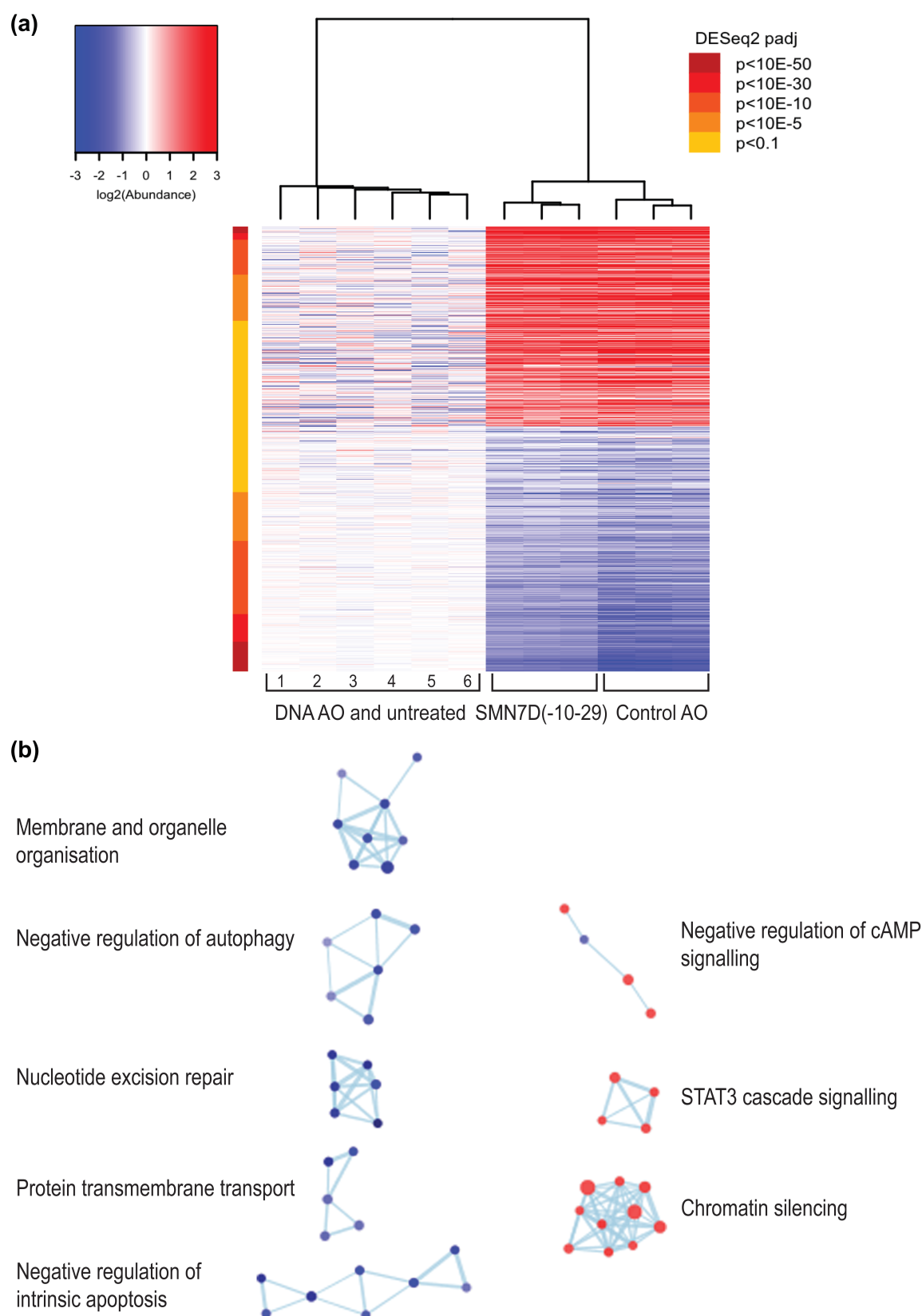530   phosphodiester oligonucleotide and untreated cells showed stark differences in expression

20

531

532

533 **Figure 6** RNA sequencing analysis of fibroblasts showing **(a)** heatmap of all differentially expressed transcripts in
534 control (1, 4, 5-untreated and 2, 3, 6, DNA AO) and 2′ O-methyl phosphorothioate AO *SMN7D(-10-20)* and
535 control AO) transfected (100 nM, 24 hours) cells, whereby red represents overexpressed transcripts, and blue

536   represents under-expressed transcripts; and **(b)** gene ontology (GO) network of significantly affected cellular
537   pathways in samples from transfected, compared to untreated and DNA AO transfected cells. GO terms are
538   represented as dots being either overexpressed (red) or under-expressed (blue), and groups with greater than
539   50% of genes in common are linked.

540

541   between the groups (**Figure 6a**). Transcripts that are overexpressed in 2′ O-methyl

542   phosphorothioate AO transfected cells compared to controls are indicated in red, while those

543   that are underexpressed are indicated in blue.

544

545   Gene ontology (GO) analyses showed significant disruptions in transcripts involved in a

546   number of major cellular pathways. The GO network (**Figure 6b**) revealed cellular processes

547   and pathways that are significantly over-expressed include signaling pathways, chromatin

548   silencing, and metabolic pathways, while those that are significantly under-expressed

549   include negative regulation of apoptosis and autophagy, membrane and organelle

550   organisation, protein transmembrane transport and nucleotide excision repair. Gene ontology

551   pathways included in each cellular process are listed in **Supplementary File 2.** Thus, overall

552   these data show dramatic and widespread changes to gene expression in human fibroblasts

553   as a result of the uptake of the 2′ O-methyl phosphorothioate AOs.

554

555   **Discussion**

556   AOs have therapeutic potential as modulators of gene expression in many different diseases,

557   and can do so through several different mechanisms. Antisense drugs that are in current

558   clinical use alter exon selection during pre-mRNA processing, or induce RNaseH degradation

559   of the target mRNA, the mechanism of action determined by the nature of the AO chemistry

560   (for review see (Tri Le *et al.* 2016)). However, emerging reports of off-target effects

561   conferred by synthetic oligonucleotides, identified *in vitro* (Shen *et al.* 2014, Shen *et al.* 2015)

562   and *in vivo* (Shen *et al.* 2014, Shen *et al.* 2018)*,* demand careful examination of the molecular

563   effects of these compounds. Here we report that transfection of cultured human dermal

564   fibroblasts, U2OS osteosarcoma cells, SH-SY5Y neuroblastoma cells and primary myogenic

565   cells with 2′ O-methyl phosphorothioate oligonucleotides causes the formation of large

566   structured nuclear inclusions, decorated with proteins that are normally components of

567   nuclear organelles, in particular, paraspeckles. We show evidence that 2′ O-methyl

568   phosphorothioate AO transfection alters the distribution of proteins normally associated with

569   subnuclear bodies, impacts on global transcript expression and ribosomal RNA processing,

570   among other critical cellular processes, and induces cell stress, followed by apoptosis.

571

572   Interaction of phosphorothioate oligonucleotides with nuclear proteins, including certain

573   paraspeckle proteins, and the formation of paraspeckle-like structures, independent of

574   *NEAT1,* has been reported (Shen *et al.* 2014, Shen *et al.* 2015, Shen *et al.* 2018). While Shen

575   *et al.* (Shen *et al.* 2014) focused on the effect of phosphorothioate AOs on NONO and

576   reported altered paraspeckle structure, this was in the context of AO-mediated modulation of

577   gene expression, not the broader cell biology. Other off-target effects and non-specific

578   binding of proteins, initiated by the negatively charged phosphorothioate backbone have

579   been reported elsewhere (Dias and Stein 2002, Winkler *et al.* 2010, Liang *et al.* 2015).

580   Hence, our experience and extensive research usage of AOs prompted further investigation of

581   the global consequences of 2´ O-methyl phosphorothioate AO transfection on cell biology,

582   showing many significant changes, as described above. In contrast, the transfection of

583   (charge-neutral) PMOs in the current study did not disrupt subnuclear structures, or result in

584   any alteration in the distribution or staining intensity of the nuclear proteins studied. This

585   result was reproducible using multiple delivery techniques, including high dose, uncomplexed

586   PMO transfection, transfection of PMO annealed to a DNA leash and complexed with

587   liposome reagent, as well as nucleofection. In comparison, all 2´ O-methyl phosphorothioate

588   AO sequences tested induced novel, structured intranuclear inclusions, revealed by

589   transmission electron microscopy to have amyloid aggregate-like appearance.

590

591   The nuclear inclusions observed in phosphorothioate transfected cells are associated with

592   altered nuclear architecture, disturbed gene expression and ultimately, apoptosis. While

593   formation of such large, and apparently irreversible structures would be expected to impact on

594   nuclear biology, the likely consequences of aberrant sequestration of paraspeckle and other

595   nuclear proteins on RNA processing and post transcriptional regulation are of prime concern.

596   Paraspeckles are dynamic, RNA-protein nuclear organelles that occur in the interchromatin

597   space in mammalian cells and are now known to contain over 40 different proteins associated

598   with one architectural long non-coding RNA, *NEAT1_2* (for review see (Fox *et al.* 2018)).

599   Observed in most cultured cells-other than various stem cells, and cells experiencing stress,

600   paraspeckles regulate gene expression through sequestration of proteins and RNAs (Fox *et al.*

601   2018), but are also implicated in microRNA biogenesis (Jiang *et al.* 2017). Paraspeckle

602   proteins can undergo rapid, but normally reversible aggregation from monomers to form

23

603   amyloid-like structures, seeded by *NEAT1_2*, and likely mediated through prion-like domains

604   that are enriched in uncharged polar amino acids (Lancaster *et al.* 2014). The mechanism by

605   which phosphorothioate oligonucleotides induce some paraspeckle proteins to form aberrant

606   aggregates is unknown, however, we do know that sub cellular localization and

607   phosphorothioate AO behaviour in transfected cells is influenced by protein interactions and

608   the 2′ sugar AO modifications (Bailey *et al.* 2017, Crooke *et al.* 2017), and that synthetic

609   double stranded RNA is also able to seed *de novo* paraspeckle formation (Shelkovnikova *et*

610   *al.* 2018). How other nuclear proteins become incorporated into the phosphorothioate AO

611   induced nuclear inclusions, and why TDP43, a major component of paraspeckles does not

612   appear in these inclusions in our study, remains elusive.

613

614   Immunofluorescent staining of 2′ O-methyl phosphorothioate transfected fibroblasts revealed

615   the paraspeckle components NONO, PSPC1, SFPQ and FUS co-localised with large nuclear

616   structures in excess of 2000 nm in length, with FUS decorating the structures in an ordered

617   manner. All four of these proteins include prion-like domains (for review see (Fox *et al.*

618   2018)) and we speculate that the known propensity of phosphorothioate backbone compounds

619   to interact with and bind proteins then alters the liquid-liquid phase properties of the

620   paraspeckle proteins, shifting them towards insoluble, amyloid-like aggregations. However,

621   not all paraspeckle components with prion-like domains investigated were found to colocalise

622   with the inclusions, and in addition, the localisation and distribution of some proteins

623   associated with other subnuclear bodies was altered in cells with nuclear inclusions.

624

625   Coilin, an integral component of Cajal bodies, nucleolin, one of the most abundant proteins in

626   the nucleolus but also found in the cytoplasm and on the cell membrane, fibrillarin, located in

627   the dense fibrillar component of the nucleolus and SC35 (SRSF2), an essential splicing factor

628   found in nuclear speckles all showed altered distribution in cells that have phosphorothioate

629   AO -induced nuclear inclusions, but did not co-localize with these inclusions. Cajal bodies

630   assemble spliceosomal and nucleolar ribonucleoproteins required for pre-mRNA and pre-

631   rRNA processing, and are recently proposed to contribute to genome organization, with global

632   effects on gene expression and RNA splicing (Wang *et al.* 2016). The nucleolus is the most

633   prominent nuclear structure, and is where synthesis and processing of ribosomal transcripts to

634   yield the mature rRNAs *5.8S, 18S* and *28S* from the *45S* pre- rRNA takes place. We show that

635   ribosomal RNA processing is greatly impaired by 2′ O-methyl phosphorothioate AO

636 transfection, and speculate that this is a likely manifestation of improper localization of major

637 protein components of the nucleolus and Cajal bodies and consequent disruption to their

638 functions. In addition, the aberrant inclusions that we speculate occupy interchromosomal

639 spaces may well impose physical constraints upon nuclear organisation, and prevent proper

640 localisation of Cajal bodies and the nucleoli close to their normal chromosomal sites. Tissues

641 with high demand for transcript splicing and ribosome biogenesis, and neurons in particular,

642 have prominent Cajal bodies, juxtaposed to nucleoli (for review see (Lafarga *et al.* 2017)),

643 and disruption or loss of Cajal bodies is associated with severe neuronal dysfunction (Tapia *et*

644 *al.* 2017). Indeed, disruption or depletion of Cajal bodies was seen as the earliest nuclear sign

645 of motor neuron degeneration in a spinal muscular atrophy mouse model and induced a

646 progressive nucleolar dysfunction in ribosome biogenesis (Tapia *et al.* 2017).

647

648 Paraspeckle biology has gained increasing interest due to the association of paraspeckle

649 proteins with neurodegenerative disease, in particular amyotrophic lateral sclerosis (ALS),

650 and the observation that *NEAT1_2* is up-regulated in early-stage motor neurons from the

651 spinal cords of ALS patients (Shelkovnikova *et al.* 2014, Yamazaki and Hirose 2015).

652 Paraspeckle formation, not observed in healthy spinal motor neurons, is enhanced in spinal

653 cords of patients with early stage sporadic and familial ALS, and mutations in many

654 paraspeckle proteins (eg. TDP-43, FUS, NONO, SFPQ) are associated with ALS (Nishimoto

655 *et al.* 2013, Shelkovnikova *et al.* 2018). Whether paraspeckles are protective or causative in

656 ALS molecular pathology is not known at this time (Yamazaki and Hirose 2015), nor is the

657 role of paraspeckles in disease well understood. Nevertheless, phosphorothioate AO-

658 mediated dysregulation of paraspeckle formation and altered nucleoli and Cajal body biology

659 shown in our study, together with the building body of evidence that nuclear organelle

660 dysfunction (Lafarga *et al.* 2017, Tapia *et al.* 2017) has implications for central nervous

661 system, and probably all, clinical applications of these compounds.

662

663 Not surprisingly, considering the altered nuclear architecture and distribution of proteins

664 implicated in RNA biology, transcriptome sequencing showed significant global effects on the

665 expression of transcripts and revealed disturbances to many critical cellular processes in

666 phosphorothioate AO transfected cells. Of particular concern, pathways involved in apoptosis,

667 chromatin silencing, cellular metabolism and a number of signalling pathways, autophagy and

668 nucleotide excision repair were disturbed. While we acknowledge that these *in vitro* studies in

25

669   replicating cells may not fully reflect potential off-target treatment effects in tissues *in vivo*,

670   Toonan et al., 2018 (Toonen *et al.* 2018) report significant upregulation of immune system-

671   associated genes in brains of mice treated by intracerebroventricular injection of 2′ O-methyl

672   phosphorothioate AO. The upregulation of immune system associated genes was detectable for

673   at least 2 months after the last AO administration.   Here, the exaggerated sequestration of

674   nuclear proteins as a result of 2′ O-methyl phosphorothioate AO transfection dramatically

675   disturbs RNA processing, disrupts nuclear architecture, and induces apoptosis, and it seems

676   reasonable to consider that injection site reactions and adverse effects reported after clinical

677   evaluation of the 2′ O-methyl phosphorothioate *Drisapersen* for the treatment of Duchenne

678   muscular dystrophy (Mendell *et al.* 2017) and *Kynamro*® (*Mipomersen*) for the treatment of

679   familial hypercholesterolemia (Wong and Goldberg 2014) may be mediated at least in part, by

680   non-specific interactions of nuclear components with the AO backbone. It might also be

681   prudent to deliberate on the reported effects of antisense drugs, attributed to the AO action on

682   the target transcript, and consider whether some level of the apparent antisense effect on

683   splicing, in particular, could perhaps be a consequence of disturbance of RNA processing

684   pathways more broadly.

685

686   We speculate that, unlike endogenous paraspeckles and other dynamic nuclear bodies, the

687   formation of the aberrant nuclear inclusions seen *in vitro* here does not appear to be

688   reversible. While 2′ O-methyl phosphorothioate transfected cultures showed reduced cell

689   numbers, whether this was due to cell death or impaired replication, or both, is uncertain, and

690   whether the nuclear inclusions *per se* or reduced availability of RNA processing are primarily

691   responsible requires further investigation. However, any effects resulting in perturbation of

692   nuclear proteins may be compounded by the formation of the nuclear amyloid-like

693   aggregates and likely disturbance of protein homeostasis, termed 'proteostasis' (Yerbury *et*

694   *al.* 2016). Although other descriptions of exogenously induced nuclear amyloid-like

695   aggregates are limited, Arnhold *et al.,* 2015 (Arnhold *et al.* 2015) identified large amyloid-

696   like aggregates in SH-SY5Y cells, treated with mercury, a notorious neurotoxicant, in a study

697   that explains the mechanism of heavy metal neurotoxicity and identified amyloid protein

698   aggregation in the cell nucleus as causative. Mass spectrometry of the purified protein

699   aggregates identified a subset of spliceosomal components and the nuclear envelope protein

700   lamin B1 (Arnhold *et al.* 2015). In our study, we also detected changes in lamin B1, although

701   here we did not detect lamin B1 in the nuclear inclusions, we nevertheless observed that

26

702   nuclear membrane and lamin B1 organization was distorted in fibroblasts containing nuclear

703   inclusions. Interestingly, the multi-lobulated nuclei and lamin B1 staining are reminiscent of

704   cells from progeria patients carrying the lamin A 433G>A mutation (E145K) (Taimen *et al.*

705   2009).

706

707 In summary, we report phosphorothioate backbone-specific effects of modified

708 oligonucleotides on the distribution and localization of nuclear proteins, appearance of novel

709 nuclear structures composed in part of a subset of paraspeckle protein components, and

710 sequence-independent effects on nascent RNA processing. While the *in vivo,* longer term

711 repercussions of exogenous oligonucleotide-induced nuclear protein aggregates that include

712 many paraspeckle components and cause sub-nuclear disorganisation are yet to be

713 determined, our observations suggest that phosphorothioate backbone antisense compounds

714 destined for clinical application would benefit from further scrutiny.

715

723

724 **Author Contributions**

725 Conceived and designed experiments: LLF, RL, SF, MTA, ILP and AF. Performed

726 experiments: LLF, RL, MTA, ILP, AH, and LG. Analysis of RNA-seq data: JC. Prepared and

727 edited manuscript: LLF, SF, RL, MTA, ILP, JC, AH, LG, SDW and AF.

728 Declaration of interests: SF and SDW act as consultants to Sarepta Therapeutics and are

729 named inventors of patents licensed through the University of Western Australia to Sarepta

730 Therapeutics. As such, they are entitled to milestone and royalty payments that may be

731 generated from licensing agreements and are involved in ongoing collaborative research

732 projects with Sarepta Therapeutics.

733
734
735

736 **References:**

737 AM Adams, PL Harding, PL Iversen, C Coleman, S Fletcher and SD Wilton (2007).
738   **Antisense oligonucleotide induced exon skipping and the dystrophin gene**
739   **transcript: Cocktails and chemistries**. *BMC Mol Biol* **8**: 57

740

741 F Arnhold, KH Guhrs and A von Mikecz (2015). **Amyloid domains in the cell nucleus**
742   **controlled by nucleoskeletal protein lamin b1 reveal a new pathway of mercury**
743   **neurotoxicity**. *PeerJ* **3**: e754.10.7717/peerj.754

744

745 JK Bailey, W Shen, XH Liang and ST Crooke (2017). **Nucleic acid binding proteins affect**
746   **the subcellular distribution of phosphorothioate antisense oligonucleotides**. *Nucleic*
747   *Acids Res* **45**(18): 10649-10671.10.1093/nar/gkx709
748

749 CF Bennett, BF Baker, N Pham, E Swayze and RS Geary (2017). **Pharmacology of**
750   **antisense drugs**. *Annu Rev Pharmacol Toxicol* **57**: 81-105.10.1146/annurev-pharmtox-
751   010716-104846
752

753 CS Bond and AH Fox (2009). **Paraspeckles: Nuclear bodies built on long noncoding rna**. *J*
754   *Cell Biol* **186**(5): 637-644.10.1083/jcb.200906113
755

756 M Chakravarthy, S Chen, PR Dodd and RN Veedu (2017). **Nucleic acid-based theranostics**
757   **for tackling alzheimer's disease**. *Theranostics* **7**(16): 3933-3947.10.7150/thno.21529
758

759 ST Crooke, S Wang, TA Vickers, W Shen and XH Liang (2017). **Cellular uptake and**
760   **trafficking of antisense oligonucleotides**. *Nat Biotechnol* **35**(3): 230-
761   237.10.1038/nbt.3779
762

763 N Dias and CA Stein (2002). **Potential roles of antisense oligonucleotides in cancer**
764   **therapy. The example of bcl-2 antisense oligonucleotides**. *Eur J Pharm Biopharm*
765   **54**(3): 263-269
766

767 S Fletcher, K Honeyman, AM Fall, PL Harding, RD Johnsen and SD Wilton (2006).
768   **Dystrophin expression in the mdx mouse after localised and systemic administration**
769   **of a morpholino antisense oligonucleotide**. *J Gene Med* **8**(2): 207-216
770

771 U Flierl, TL Nero, B Lim, JF Arthur, Y Yao, SM Jung, E Gitz, AY Pollitt, MT Zaldivia, M
772   Jandrot-Perrus, A Schafer, B Nieswandt, RK Andrews, MW Parker, EE Gardiner and K
773   Peter (2015). **Phosphorothioate backbone modifications of nucleotide-based drugs**
774   **are potent platelet activators**. *J Exp Med* **212**(2): 129-137.10.1084/jem.20140391
775

776 AH Fox, S Nakagawa, T Hirose and CS Bond (2018). **Paraspeckles: Where long noncoding**
777   **rna meets phase separation**. *Trends Biochem Sci* **43**(2): 124-
778   135.10.1016/j.tibs.2017.12.001
779

780 BL Gebski, CJ Mann, S Fletcher and SD Wilton (2003). **Morpholino antisense**
781   **oligonucleotide induced dystrophin exon 23 skipping in mdx mouse muscle**. *Hum*
782   *Mol Genet* **12**(15): 1801-1811
783

784 L Jiang, C Shao, QJ Wu, G Chen, J Zhou, B Yang, H Li, LT Gou, Y Zhang, Y Wang, GW Yeo,
785   Y Zhou and XD Fu (2017). **Neat1 scaffolds rna-binding proteins and the**
786   **microprocessor to globally enhance pri-mirna processing**. *Nat Struct Mol Biol* **24**(10):
787   816-824.10.1038/nsmb.3455
788

789 M Kinali, V Arechavala-Gomeza, L Feng, S Cirak, D Hunt, C Adkin, M Guglieri, E Ashton, S
790   Abbs, P Nihoyannopoulos, ME Garralda, M Rutherford, C McCulley, L Popplewell, IR
791   Graham, G Dickson, MJ Wood, DJ Wells, SD Wilton, R Kole, V Straub, K Bushby, C
792   Sewry, JE Morgan and F Muntoni (2009). **Local restoration of dystrophin expression**
793   **with the morpholino oligomer avi-4658 in duchenne muscular dystrophy: A single-**

794   **blind, placebo-controlled, dose-escalation, proof-of-concept study**. *Lancet Neurol*
795   **8**(10): 918-928.S1474-4422(09)70211-X [pii] 10.1016/S1474-4422(09)70211-X
796

797   M Lafarga, O Tapia, AM Romero and MT Berciano (2017). **Cajal bodies in neurons**. *RNA*
798   *Biol* **14**(6): 712-725.10.1080/15476286.2016.1231360
799

800   AK Lancaster, A Nutter-Upham, S Lindquist and OD King (2014). **Plaac: A web and**
801   **command-line application to identify proteins with prion-like amino acid**
802   **composition**. *Bioinformatics* **30**(17): 2501-2502.10.1093/bioinformatics/btu310
803

804   R Li, AR Harvey, SI Hodgetts and AH Fox (2017). **Functional dissection of neat1 using**
805   **genome editing reveals substantial localization of the neat1_1 isoform outside**
806   **paraspeckles**. *RNA* **23**(6): 872-881.10.1261/rna.059477.116
807

808   S Li, FJ Shu, Z Li, L Jaafar, S Zhao and WS Dynan (2017). **Cell-type specific role of the**
809   **rna-binding protein, nono, in the DNA double-strand break response in the mouse**
810   **testes**. *DNA Repair (Amst)* **51**: 70-78.10.1016/j.dnarep.2017.02.002
811

812   XH Liang, H Sun, W Shen and ST Crooke (2015). **Identification and characterization of**
813   **intracellular proteins that bind oligonucleotides with phosphorothioate linkages**.
814   *Nucleic Acids Res* **43**(5): 2927-2945.10.1093/nar/gkv143
815

816   F Lipi, S Chen, M Chakravarthy, S Rakesh and RN Veedu (2016). **In vitro evolution of**
817   **chemically-modified nucleic acid aptamers: Pros and cons, and comprehensive**
818   **selection strategies**. *RNA Biol* **13**(12): 1232-1245.10.1080/15476286.2016.1236173
819

820   JR Mendell, N Goemans, LP Lowes, LN Alfano, K Berry, J Shao, EM Kaye, E Mercuri, G
821   Eteplirsen Study and DMDIN Telethon Foundation (2016). **Longitudinal effect of**
822   **eteplirsen versus historical control on ambulation in duchenne muscular dystrophy**.
823   *Ann Neurol* **79**(2): 257-271.10.1002/ana.24555
824

825   JR Mendell, LR Rodino-Klapac, Z Sahenk, K Roush, L Bird, LP Lowes, L Alfano, AM
826   Gomez, S Lewis, J Kota, V Malik, K Shontz, CM Walker, KM Flanigan, M Corridore, JR
827   Kean, HD Allen, C Shilling, KR Melia, P Sazani, JB Saoud, EM Kaye and G Eteplirsen
828   Study (2013). **Eteplirsen for the treatment of duchenne muscular dystrophy**. *Ann*
829   *Neurol* **74**(5): 637-647.10.1002/ana.23982
830

831   JR Mendell, Z Sahenk and L Rodino-Klapac (2017). **Clinical trials of exon skipping in**
832   **duchenne muscular dystrophy**. *Expert Opinion on Orphan Drugs* **5**(9): 683-690.DOI:
833   10.1080/21678707.2017.1366310
834

835   C Mitrpant, P Porensky, H Zhou, L Price, F Muntoni, S Fletcher, SD Wilton and AH Burghes
836   (2013). **Improved antisense oligonucleotide design to suppress aberrant smn2 gene**
837   **transcript processing: Towards a treatment for spinal muscular atrophy**. *PLoS One*
838   **8**(4): e62114.10.1371/journal.pone.0062114
839

840   T Naganuma, S Nakagawa, A Tanigawa, YF Sasaki, N Goshima and T Hirose (2012).
841   **Alternative 3'-end processing of long noncoding rna initiates construction of nuclear**
842   **paraspeckles**. *EMBO J* **31**(20): 4020-4034.10.1038/emboj.2012.251
843

844   Y Nishimoto, S Nakagawa, T Hirose, HJ Okano, M Takao, S Shibata, S Suyama, K Kuwako,
845   T Imai, S Murayama, N Suzuki and H Okano (2013). **The long non-coding rna nuclear-**
846   **enriched abundant transcript 1_2 induces paraspeckle formation in the motor**
847   **neuron during the early phase of amyotrophic lateral sclerosis**. *Mol Brain* **6**:
848   31.10.1186/1756-6606-6-31
849
850   DM Paton (2017). **Nusinersen: Antisense oligonucleotide to increase smn protein**
851   **production in spinal muscular atrophy**. *Drugs Today (Barc)* **53**(6): 327-
852   337.10.1358/dot.2017.53.6.2652413
853
854   TA Shelkovnikova, MS Kukharsky, H An, P Dimasi, S Alexeeva, O Shabir, PR Heath and VL
855   Buchman (2018). **Protective paraspeckle hyper-assembly downstream of tdp-43 loss**
856   **of function in amyotrophic lateral sclerosis**. *Mol Neurodegener* **13**(1):
857   30.10.1186/s13024-018-0263-7
858
859   TA Shelkovnikova, HK Robinson, C Troakes, N Ninkina and VL Buchman (2014).
860   **Compromised paraspeckle formation as a pathogenic factor in fusopathies**. *Human*
861   *Molecular Genetics* **23**(9): 2298-2312.10.1093/hmg/ddt622
862
863   L Shen, A Frazer-Abel, PR Reynolds, PC Giclas, A Chappell, MK Pangburn, H Younis and SP
864   Henry (2014). **Mechanistic understanding for the greater sensitivity of monkeys to**
865   **antisense oligonucleotide-mediated complement activation compared with humans**.
866   *J Pharmacol Exp Ther* **351**(3): 709-717.10.1124/jpet.114.219378
867
868   W Shen, CL De Hoyos, H Sun, TA Vickers, XH Liang and ST Crooke (2018). **Acute**
869   **hepatotoxicity of 2' fluoro-modified 5-10-5 gapmer phosphorothioate**
870   **oligonucleotides in mice correlates with intracellular protein binding and the loss of**
871   **dbhs proteins**. *Nucleic Acids Res* **46**(5): 2204-2217.10.1093/nar/gky060
872
873   W Shen, XH Liang and ST Crooke (2014). **Phosphorothioate oligonucleotides can displace**
874   **neat1 rna and form nuclear paraspeckle-like structures**. *Nucleic Acids Res* **42**(13):
875   8648-8662.10.1093/nar/gku579
876
877   W Shen, XH Liang, H Sun and ST Crooke (2015). **2'-fluoro-modified phosphorothioate**
878   **oligonucleotide can cause rapid degradation of p54nrb and psf**. *Nucleic Acids Res*
879   **43**(9): 4569-4578.10.1093/nar/gkv298
880
881   NK Singh, NN Singh, EJ Androphy and RN Singh (2006). **Splicing of a critical exon of**
882   **human survival motor neuron is regulated by a unique silencer element located in**
883   **the last intron**. *Mol Cell Biol* **26**(4): 1333-1346.10.1128/MCB.26.4.1333-1346.2006
884
885   CA Stein and D Castanotto (2017). **Fda-approved oligonucleotide therapies in 2017**. *Mol*
886   *Ther* **25**(5): 1069-1075.10.1016/j.ymthe.2017.03.023
887
888   P Taimen, K Pfleghaar, T Shimi, D Moller, K Ben-Harush, MR Erdos, SA Adam, H
889   Herrmann, O Medalia, FS Collins, AE Goldman and RD Goldman (2009). **A progeria**
890   **mutation reveals functions for lamin a in nuclear assembly, architecture, and**
891   **chromosome organization**. *Proc Natl Acad Sci U S A* **106**(49): 20788-
892   20793.10.1073/pnas.0911895106
893

O Tapia, JO Narcis, J Riancho, O Tarabal, L Piedrafita, J Caldero, MT Berciano and M Lafarga (2017). **Cellular bases of the rna metabolism dysfunction in motor neurons of a murine model of spinal muscular atrophy: Role of cajal bodies and the nucleolus**. *Neurobiol Dis* **108**: 83-99.10.1016/j.nbd.2017.08.004

LJA Toonen, J Casaca-Carreira, M Pellise-Tintore, H Mei, Y Temel, A Jahanshahi and WMC van Roon-Mom (2018). **Intracerebroventricular administration of a 2'-o-methyl phosphorothioate antisense oligonucleotide results in activation of the innate immune system in mouse brain**. *Nucleic Acid Ther* **28**(2): 63-73.10.1089/nat.2017.0705

B Tri Le, RN Veedu, S Fletcher and SD Wilton (2016). **Antisense oligonucleotide development for the treatment of muscular dystrophies**. *Expert Opinion on Orphan Drugs* **4**(2): 139-152.10.1517/21678707.2016.1122517

RN Veedu (2015). **Medicinal chemistry of aptamers**. *Curr Top Med Chem* **15**(12): 1065

Q Wang, IA Sawyer, MH Sung, D Sturgill, SP Shevtsov, G Pegoraro, O Hakim, S Baek, GL Hager and M Dundr (2016). **Cajal bodies are linked to genome conformation**. *Nat Commun* **7**: 10966.10.1038/ncomms10966

SD Wilton, RN Veedu and S Fletcher (2015). **The emperor's new dystrophin: Finding sense in the noise**. *Trends Mol Med* **21**(7): 417-426.10.1016/j.molmed.2015.04.006

J Winkler, M Stessl, J Amartey and CR Noe (2010). **Off-target effects related to the phosphorothioate modification of nucleic acids**. *ChemMedChem* **5**(8): 1344-1352.10.1002/cmdc.201000156

E Wong and T Goldberg (2014). **Mipomersen (kynamro): A novel antisense oligonucleotide inhibitor for the management of homozygous familial hypercholesterolemia**. *P T* **39**(2): 119-122

T Yamazaki and T Hirose (2015). **The building process of the functional paraspeckle with long non-coding rnas**. *Front Biosci (Elite Ed)* **7**: 1-41

JJ Yerbury, L Ooi, A Dillin, DN Saunders, DM Hatters, PM Beart, NR Cashman, MR Wilson and H Ecroyd (2016). **Walking the tightrope: Proteostasis and neurodegenerative disease**. *Journal of Neurochemistry* **137**(4): 489-505.10.1111/jnc.13575

934